ASTRA MODELING OF ELECTRON CYCLOTRON HEATING IN THE HELICALLY SYMMETRIC EXPERIMENT

JOSEPH N. TALMADGE,* KONSTANTIN M. LIKIN, ALI EL-SAYED ALI ABDOU, ABDULGADER F. ALMAGRI, DAVID T. ANDERSON, F. SIMON B. ANDERSON, JOHN M. CANIK, CHUANBAO DENG, STEFAN P. GERHARDT, and KAN ZHAI
The HSX Plasma Laboratory, University of Wisconsin-Madison, Madison, Wisconsin 53704

Received November 18, 2003
Accepted for Publication March 31, 2004

Thomson scattering and diamagnetic loop measurements in a hot electron plasma in the Helically Symmetric Experiment (HSX) indicate that the central electron temperature and stored energy increase linearly with power. Experimentally it is found that the central electron temperature is roughly independent of plasma density. The ASTRA code is used to model electron cyclotron heating for a magnetic configuration that is quasi-symmetric as well as for a configuration in which the symmetry is broken. The experimental results are consistent with an anomalous thermal conductivity that scales inversely with the density. However, the experimental scaling of the stored energy against density is not usually in agreement with the model. From the measured X-ray flux and the high absorbed power, as well as from the calculated low single-pass absorption efficiency, it is concluded that at low densities, a nonthermal electron population accounts for a significant fraction of the stored energy. With the ASTRA code, it is also possible to model under what conditions the central electron temperature in the quasi-symmetric configuration will be measurably greater than the temperature in the nonsymmetric configuration. These calculations depend greatly on the radial electric field of the nonsymmetric plasma but suggest that at somewhat higher density and higher power than achieved to date, differences in the central electron temperature may be observed.

KEYWORDS: *ECH, HSX, transport*

I. INTRODUCTION

Plasma heating in the Helically Symmetric Experiment (HSX) is done at a magnetic field of 0.5 T using the extraordinary wave at the second harmonic of the electron cyclotron frequency. To investigate the improved confinement properties of the quasi-helically symmetric configuration, a 28-GHz gyrotron is used to heat electrons into the low-collisionality regime. So far, up to 100 kW has been launched from the low-field side of the device in the form of a Gaussian beam. In HSX, neoclassical transport can be greatly increased with a set of auxiliary coils that adds a toroidal Mirror term to the magnetic field spectrum. In the Mirror configuration, the field is increased at the location of the microwave antenna, while in the anti-Mirror configuration the field is decreased. For all configurations, the magnetic field on the magnetic axis is kept at 0.5 T so that the axis is resonant with the gyrotron frequency unless the intention is to perform off-axis heating. Trapped particles are well confined for the quasi-helically symmetric (QHS) configuration, while they are lost from the outboard side of the torus at the location of the antenna in the Mirror configuration. However, trapped particles launched near the antenna for the anti-Mirror configuration are lost from both the inboard and outboard sides of the torus.

II. NEOCLASSICAL TRANSPORT AND POWER DEPOSITION PROFILE

Electron cyclotron heating (ECH) in HSX is modeled by using the ASTRA code.[1] The neoclassical contribution to the transport is determined by using a Monte

*E-mail: talmadge@facstaff.wisc.edu

Carlo code to calculate the monoenergetic diffusion coefficient on a particular flux surface. The data are then fit to an analytic expression that consists of the sum of symmetric and asymmetric transport. The tokamak-like symmetric transport is given by an analytic expression formulated by Beidler and Hitchon.[2] The asymmetric contribution to the transport is fit to a six-parameter analytic expression originally developed by Shaing[3] and later modified by Painter and Gardner.[4] The expression, which spans a wide range of collisionalities and is valid for both large and small electric fields, is written in the following manner:

$$
\begin{aligned}
D &= \frac{\sqrt{\pi}}{2}\,\varepsilon_t\sqrt{C_6}V_d^2\,\frac{\nu}{\omega^2} \ , \\
\omega^2 &= C_1\tilde{\nu}^2 + C_2(\omega_E+\omega_B)^2 + C_3\omega_B^2 + C_4|\omega_B|\tilde{\nu} \ , \\
\omega_B &= -C_5V_d \ , \\
V_d &= \frac{K}{eBr} \ , \\
\tilde{\nu} &= \frac{\nu}{C_6} \ , \\
\omega_E &= \frac{E}{rB} \ , \\
\varepsilon_t &= r/R \ .
\end{aligned}
\tag{1}
$$

This simple form of the monoenergetic diffusion coefficient fits the Monte Carlo data over a broad range of electric fields, magnetic fields, collisionality, particle energy, and particle mass. The coefficients C_1 to C_6 are calculated for five radial locations that span the plasma minor radius and are then interpolated to obtain the diffusion coefficients in the intermediate regions. The particle and heat fluxes in ASTRA for a given species j, including the off-diagonal terms, are calculated by taking moments of the monoenergetic diffusion coefficient:

$$\Gamma_j = -D_1 n_j\left\{\frac{n_j'}{n_j} - \frac{q_j E_r}{T_j} + \left(\frac{D_2}{D_1} - 3/2\right)\frac{T_j'}{T_j}\right\} \tag{2}$$

and

$$Q_j = -D_2 n_j T_j\left\{\frac{n_j'}{n_j} - \frac{q_j E_r}{T_j} + \left(\frac{D_3}{D_2} - 3/2\right)\frac{T_j'}{T_j}\right\} \ , \tag{3}$$

where

$$
\begin{aligned}
D_{n,j} &= \frac{2}{\sqrt{\pi}}\int_0^\infty dx_j\cdot x_j^{(2n-1)/2}D(x_j)\cdot\exp(-x_j) \ , \\
x_j &= \frac{m_j v^2}{2T_j}
\end{aligned}
\tag{4}
$$

is the normalized energy and $D(x_j)$ is the monoenergetic diffusion coefficient. One important advantage of using the analytic fits to the Monte Carlo data is that it provides a fast way of calculating the ambipolar radial electric field by setting the ion and electron fluxes equal to each other: $\Gamma_i(r,E_r) = \Gamma_e(r,E_r)$, where r is a flux surface label.

The power deposition profile for the ASTRA code is based on a combination of ray-tracing calculations and experimental measurements. A series of waveguide mode converters in the transmission line takes the hollow power density profile of the TE02 output of the gyrotron and transforms it to a Gaussian-like profile in the HE11 mode. An ellipsoidal Mirror focuses the microwave power onto the magnetic axis with a beam diameter of 4 cm. The output spot size has been measured experimentally and compares well with the design parameters. Using the appropriate beam width and curvature radius at the plasma boundary, a ray-tracing code was used to compute the power deposition profile in the plasma.[5] For the ASTRA code, we assume a deposition profile somewhat larger than the calculation: $P = P_0\,[1-(r/a)^2]^{40}$. The total integrated absorbed power is determined by the decay of the stored energy as measured by a diamagnetic loop. Experimentally, the absorbed power based on the loop measurements is a relatively insensitive function of the plasma density for line-average densities greater than 0.5×10^{18} m^{-3}. This result is further confirmed by measurements of the multipass absorption efficiency (absorbed power/input power) with a set of microwave diodes. For the purpose of modeling the temperature dependence on the plasma density, we have assumed therefore that the absorbed power is independent of density for a given input power.

III. ELECTRON TEMPERATURE SCALING

The density profile in HSX, which tends to be peaked, is measured with a nine-chord interferometer. We used the experimental density profile in ASTRA while solving for the ion and electron temperatures, given the power deposition profile. Since electron transport in stellarators is typically not solely neoclassical, the electron thermal conductivity in the ASTRA calculation was specified as the sum of a neoclassical term plus an anomalous component. Previously, to estimate what electron temperatures we might expect in HSX during ECH at 0.5 T (Ref. 6), we used an anomalous thermal conductivity given by a form of the ASDEX L-mode scaling law that reproduces the experimental profiles in Wendelstein 7-AS (Ref. 1). The thermal conductivity in this model is proportional to $T_e^{3/2}$ and yields a dependence of the temperature on the density and power, $T\sim(P/n)^{0.4}$ and a stored energy that goes as $W\sim n^{0.6}P^{0.4}$.

Recently the central channel of a 10-channel Thomson scattering system with a Nd:YAG laser has been made operational. As seen in Fig. 1, the central temperature is roughly independent of density, except perhaps at the lowest densities for the QHS configuration. These data are with a constant input power of 40 kW. Figure 2 shows the central electron temperature for a fixed average density of 1.5×10^{18} m^{-3}, as the gyrotron power is varied from 20 to 100 kW. It can be seen from the figure that for the QHS configuration, the central T_e appears to scale linearly with power. The two scaling results indicate that the ASDEX L-mode model for the anomalous thermal conductivity does not follow the experimental scaling.

Instead we find better agreement with the experimental data for an anomalous thermal conductivity that scales as $\chi_{e,an} = 10.35/n_e$, where the conductivity is in units of m^2/s and the density is in units of 10^{18} m^{-3}. This gives a temperature dependence that is independent of density and linear with power. Modeling of the particle diffusion coefficient based on calibrated H_α measurements and DEGAS calculations gives a similar dependence on the plasma density.[7] This sort of Alcator-like dependence for the thermal conductivity was found to be a good fit to the data for the early Heliotron-E ECH results with a 28-GHz gyrotron.[8] In Figs. 1 and 2 are also plotted the ASTRA calculation of the central electron temperature for the QHS and Mirror configurations. For the QHS configuration, the transport is determined by anomalous transport since the neoclassical fluxes are so low. For the Mirror configuration, however, two curves are plotted, corresponding to the case when the radial electric field is set to zero, as well as when the ambipolar electric field is determined. For the latter case, the radial electric field is given by the electron root of the ambipolarity condition. With a positive electric field on the order of 90 V/cm, the electron flux is decreased considerably for the Mirror and makes the transport properties of this configuration similar to the QHS mode of operation. However, as discussed by Maassberg et al.,[9] the expected confinement improvement due to the electron root was not observed in medium-size experiments similar to HSX, even when the theory predicted such a root should be present. The theoretical prediction of an electron root may be too optimistic. One may then expect the experimental measurement of the central electron temperature for the Mirror configuration to be bounded by a calculation that assumes either zero electric field or the ambipolar field. At this time, there are insufficient data to distinguish which of the two predictions for the Mirror configuration might best approximate the experimental results.

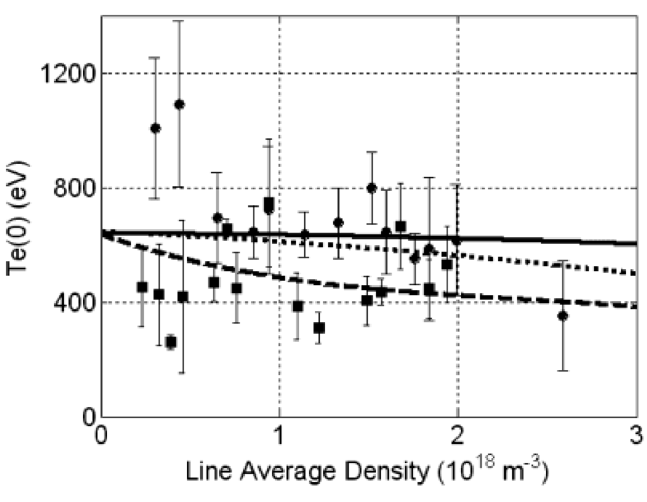

Fig. 1. Central electron temperature measured by Thomson scattering as a function of line average density for QHS (circles) and Mirror (squares) configurations. Also shown are the ASTRA calculations for the QHS (solid line) and Mirror modes ($E_r = 0$, dashed line; ambipolar E_r, dotted line).

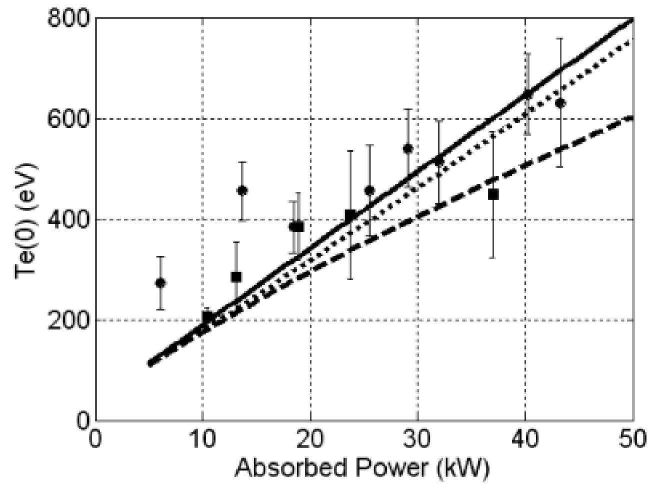

Fig. 2. Central T_e compared with absorbed power from Thomson scattering for QHS (circles) and Mirror (squares) configurations, as well as ASTRA calculation for QHS (solid) and Mirror modes ($E_r = 0$, dashed line; ambipolar E_r, dotted line).

IV. STORED ENERGY SCALING

Figure 3 shows that the stored energy increases linearly as a function of the absorbed power for the QHS and Mirror configurations at a fixed density of 1.5×10^{18} m^{-3}. The absorbed power is calculated based on the difference of the slopes in the stored energy before and after the gytrotron turn-off. This linear dependence is in agreement with the Alcator-like model for anomalous transport, rather than the ASDEX L-mode model. The difference between the QHS and Mirror stored energy reflects the 15% lower plasma volume for the Mirror case. From the figure, it can be seen that only at the higher powers does the stored energy agree with ISS95

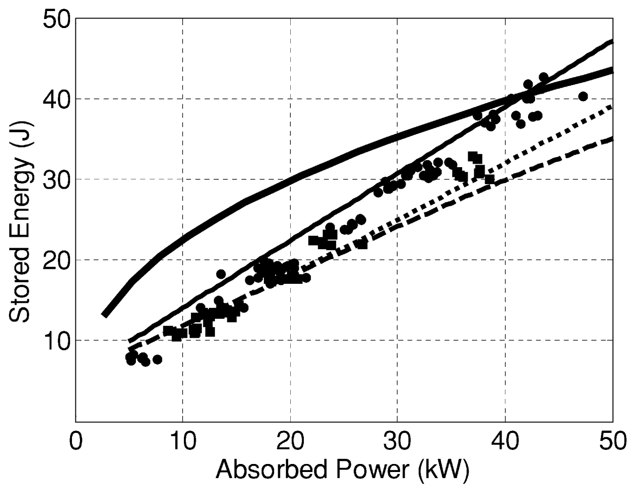

Fig. 3. Stored energy from diamagnetic loop versus absorbed power for QHS (circles) and Mirror (squares) configurations, as well as ASTRA calculation for QHS (solid) and Mirror modes ($E_r = 0$, dashed line; ambipolar E_r, dotted line). Also shown is the stored energy based on ISS95 scaling (heavy line).

scaling,[10] although the functional dependence on the power is very different.

We would expect from the Alcator-like model that for fixed input power, the stored energy should increase linearly with the plasma density. Figure 4 shows, however, that for a constant input power of 40 kW, this is not so for central resonance heating in both the QHS and Mirror configurations. (Note that above $\sim 2.5 \times 10^{18}\ \mathrm{m}^{-3}$, the stored energy falls as the central density approaches cutoff.) In contrast, Fig. 5 shows that for Mirror outboard resonance at $r/a = 0.5$, where confinement of trapped electrons is poor, the linear dependence of the stored energy on the density does agree with the model.

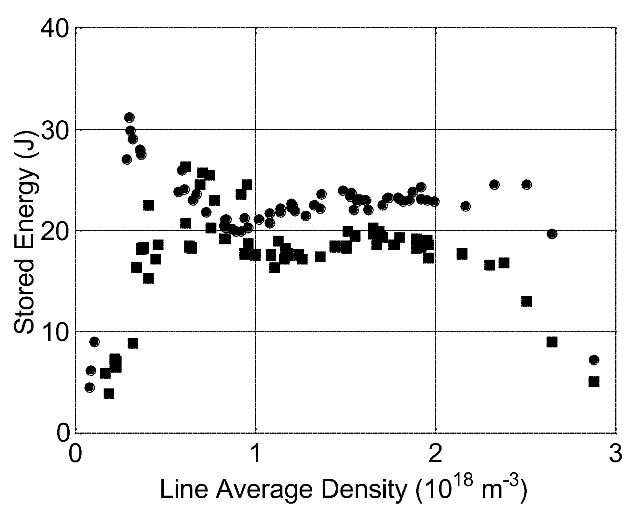

Fig. 4. Stored energy compared with line average density for QHS (circles) and Mirror (squares) central resonance heating.

To understand why the dependence of the stored energy on the density does not agree with the model under most circumstances, we measured the hard X-ray emission from the plasma by using a collimated CdZnTl detector. Figure 6 shows that the emission increases with density to a maximum at $0.5 \times 10^{18}\ \mathrm{m}^{-3}$ and then falls off sharply at higher densities. Similarly, the stored energy also shows a peak at $0.5 \times 10^{18}\ \mathrm{m}^{-3}$ but remains roughly constant at higher densities. The conclusion from this comparison of the X-ray emission with the stored

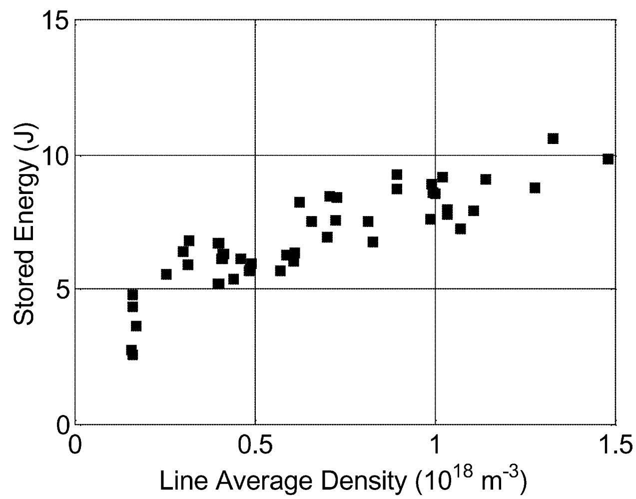

Fig. 5. Stored energy compared with line average density for Mirror outboard resonance at $r/a = 0.5$.

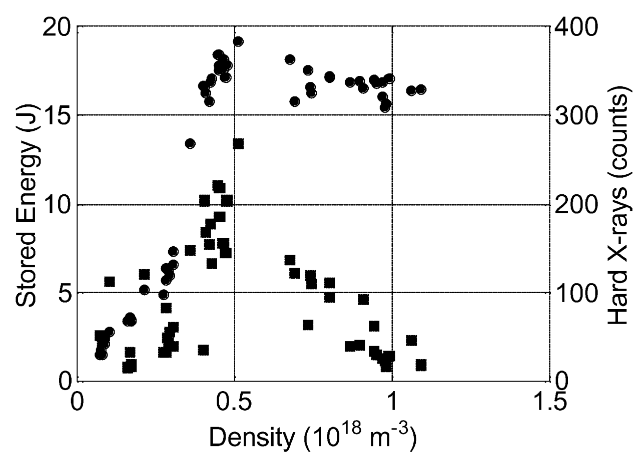

Fig. 6. Hard X-ray counts (squares) and stored energy (circles) as a function of line average density for Mirror central resonance.

energy is that a nonthermal component in the plasma makes a significant contribution to the stored energy at the lower densities.

V. RAY TRACING AND ABSORBED POWER

This existence of a nonthermal component is further supported by a comparison of the absorption efficiency from a ray-tracing code with measurements of the absorbed power.[5] Figure 7 shows the results of the ray-tracing calculation. The single-pass absorption is calculated assuming a parabolic density profile and an exponential electron temperature profile. With a central temperature assumed to be 0.4 keV, the single-pass absorption coefficient is 0.4 at a line average density of 1.5×10^{18} m^{-3}. Using the Thomson scattering data for the central temperature and a bi-Maxwellian distribution based on electron cyclotron emission, there is more absorption at the lower densities. However, both calculations show that the absorption efficiency should increase with density up to the cutoff at a line average density of 3×10^{18} m^{-3}. Calculations of multipass absorption indicate that the total absorption efficiency can be as high as 70% for two passes.

Figure 8 shows the measured multipass absorption efficiency compared with plasma density for the QHS and Mirror configurations. The efficiency is measured by using a set of microwave antennas, four of which are plotted in the figure. For both configurations, the efficiency is in the range of 0.8 to 0.98. It can be seen that for the Mirror configuration, the efficiency drops at densities less than 0.5×10^{18} m^{-3}, while for the QHS configuration it remains high. Interestingly, for the anti-Mirror configuration, in which the confinement of trapped particles near the ECH antenna is the worst of the three

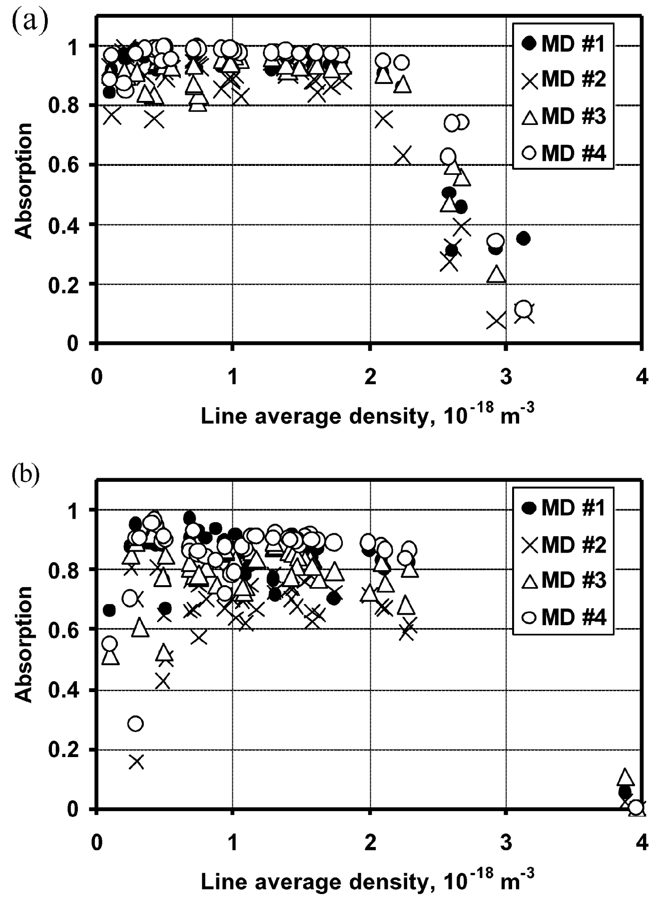

Fig. 8. Measured absorption coefficients for (a) QHS and (b) Mirror configurations measured by microwave antennas.

configurations, the measured multipass absorption efficiency is never higher than 0.6, while the stored energy remains low at only 5 to 7 J. For this configuration, there are no hard X-rays even at the lowest densities. Hence, the discrepancy between the ray-tracing calculations and measured high multipass absorption efficiency at low plasma density is most likely due to additional absorption on a nonthermal electron population. Furthermore, the differences in absorption measured for the QHS, Mirror, and anti-Mirror configurations can be explained by differences in trapped particle confinement.

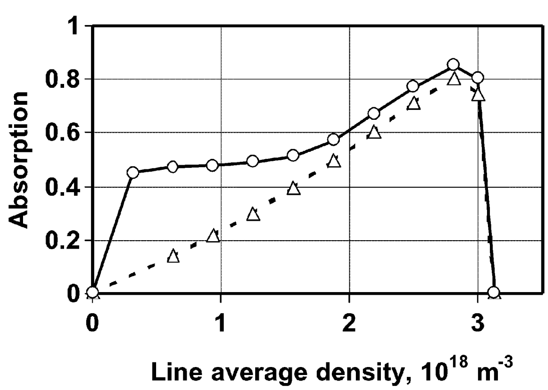

Fig. 7. Ray-tracing calculation of absorption efficiency compared with line average density, assuming constant peak temperature of 0.4 keV (triangles) and from a bi-Maxwellian plasma based on temperatures from Thomson scattering and electron cyclotron emission (circles).

VI. CONCLUSION

In summary, anomalous transport in HSX is best described by an Alcator-like thermal conductivity in which the conductivity is inversely proportional to the density. Departures of the experimental results from this model, as with the measured stored energy as a function of plasma density, can best be explained by a nonthermal component of the electron distribution that is accounting for a significant fraction of the stored energy. In the ASTRA modeling of ECH plasmas in HSX that has been done so far, we have not considered how much of the absorbed power goes to the bulk plasma and how much to the nonthermal population. It is possible that the Alcator-like scaling of the anomalous thermal conductivity may be dependent on the existence of this nonthermal population. Future work using a Fokker-Planck code will explore further the role of the nonthermal population and improve the modeling of these two-component plasmas.

One of the goals of HSX is to investigate whether the reduced neoclassical transport of the quasi-helical configuration compared with a conventional stellarator can lead to observable differences in plasma parameters. The initial modeling done here suggests that anomalous transport may overwhelm differences in neoclassical transport, but that by operating at higher density and higher power than achieved to date, the central electron temperature may differ between the QHS and Mirror configurations. The magnitude of that difference, however, depends strongly on the radial electric field.

ACKNOWLEDGMENT

This work is supported by U.S. Department of Energy grant DE-FG02-93ER54222.

REFERENCES

1. N. KARULIN, "Transport Modeling of Stellarators with ASTRA," IPP 2/328 (Dec. 1994).

2. C. D. BEIDLER and W. N. G HITCHON, "Ripple Transport in Helical-Axis Advanced Stellarators: A Comparison with Classical Stellarator/Torsatrons," *Plasma Phys. Contr. Fusion*, **36**, 317 (1994).

3. K. C. SHAING, "Stability of the Radial Electric Field in a Nonaxisymmetric Torus," *Phys. Fluids*, **27**, 1567 (1984).

4. S. L. PAINTER and H. J. GARDNER, "Orbit Confinement and Neoclassical Transport in the H-1 Heliac," *Nucl. Fusion*, **33**, 1107 (1993).

5. K. LIKIN et al., "Comparison of Electron Cyclotron Heating Results in the Helically Symmetric Experiment with and without Quasi-Symmetry," *Plasma Phys. Contr. Fusion*, **45**, A133 (2003).

6. J. N. TALMADGE et al., "Transport in HSX Electron Cyclotron Heated Plasmas at 0.5 T," presented at 13th Int. Stellarator Workshop, Canberra, Australia (2002).

7. J. CANIK et al., "Particle Neutral Density Modeling and Measurements in HSX," presented at 14th Int. Stellarator Workshop, Greifswald, Germany (2003).

8. H. ZUSHI et al., "Transport Simulation of the Currentless ECRH Plasma in Heliotron E," *Nucl. Fusion*, **24**, 305 (1984).

9. H. MAASSBERG et al., "Experimental and Neoclassical Electron Heat Transport in the LMFP Regime for the Stellarators W7-A, L-2, and W7-AS," *Phys. Fluids B*, **5**, 3627 (1993).

10. U. STROTH, M. MURAKAMI, R. A. DORY, H. YAMADA, S. OKAMURA, F. SANO, and T. OBIKI, "Energy Confinement Scaling from the International Stellarator Database," *Nucl. Fusion*, **36**, 1063 (1996).

Joseph N. Talmadge (BS, applied physics, Columbia University, 1974; PhD, physics, University of Wisconsin, 1982) is an associate scientist in the Electrical and Computer Engineering (ECE) department at the University of Wisconsin-Madison. His current research interests are in stellarator physics, plasma heating, confinement and transport, plasma flow damping, electric fields and computer modeling.

Konstantin M. Likin (BS, radio physics and electronics, Gorky State University, Gorky, Russia, 1979; Msci, electrodynamics, Institute of Applied Physics, Gorky, 1980; PhD, plasma physics, General Physics Institute, Moscow, 1994) is an associate scientist in the ECE department at the University of Wisconsin-Madison. His current responsibilities and research interests are in electron cyclotron resonance heating (ECRH) experiments on the Helically Symmetric Experiment (HSX) stellarator, plasma heating by electron cyclotron waves, microwave diagnostics and numerical modeling of ECRH, and ECE in three-dimensional toroidal geometry.

Ali El-Sayed Ali Abdou (BS, nuclear engineering, Alexandria University, Egypt, 1992; MSc, nuclear engineering, 2002; and MSc, computational sciences, 2003, University of Wisconsin-Madison) is a graduate student in the Department of Engineering Physics at the University of Wisconsin-Madison. His current research interests are in stellarator physics, X-ray measurements, and Fokker-Planck modeling.

Abdulgader F. Almagri (BS, 1981, and PhD, 1990, physics, University of Wisconsin-Madison) is an associate scientist in the ECE and Physics Departments of the University of Wisconsin-Madison. His interests are in magnetic fluctuations and turbulence, X-ray measurements, particle confinement, magnetohydodynamic and Hall dynamo activities, as well as plasma flows and momentum damping.

David T. Anderson (BS, 1974; MS, 1975; and PhD, 1985, electrical and computer engineering, University of Wisconsin-Madison) is an associate professor in the ECE department at the University of Wisconsin-Madison. His research interests are confinement and heating in stellarator systems and modular stellarator design.

F. Simon B. Anderson (BSc, physics, 1976; and BSc Hons 1A, plasma physics, 1977; and PhD, plasma physics, 1981, Flinders University of South Australia) is an associate scientist in the ECE department at the University of Wisconsin-Madison. His current responsibilities and research interests are in optical and particle diagnostics, operational and upgrade support for the HSX device and computer systems, and stellarator transport and confinement.

John M. Canik (BA, physics and computer science, New York University, 2001) is a graduate student in the ECE department at the University of Wisconsin-Madison. His research interests are particle transport, spectroscopy, and computer modeling.

Chuanbao Deng (BS, physics, Shandong University, 1982; Msci, physics, Institute of Plasma Physics, Chinese Academy of Sciences, 1986; PhD, physics, Flinders University, Australia, 1999) is an assistant development engineer in the Electrical Engineering department at the University of California-Los Angeles. His current responsibilities are the design, fabrication, and operation of a multichannel interferometer system on HSX. His research interests are in high-temperature diagnostics, stellarator physics, particle transport, and plasma fluctuations.

Stefan P. Gerhardt (BS, applied math, engineering, and physics, 1998, and MS, electrical engineering, 2001, University of Wisconsin-Madison) is a graduate student in the ECE department at the University of Wisconsin-Madison. His current research interests are in neoclassical transport, plasma flow damping, and spectroscopy.

Kan Zhai (BS, physics, 1989, and PhD, physics, 1995, University of Science and Technology of China) is an assistant scientist in the ECE department at the University of Wisconsin-Madison. His current responsibilities are the design, construction, and operation of a multichannel Thomson scattering diagnostic for HSX. His research interests are in plasma diagnostics, instabilities, and transport.